analytical chemistry

pubs.acs.org/ac

Article

Ultrasensitive Detection and In Situ Imaging of Analytes on Graphene Oxide Analogues Using Enhanced Raman Spectroscopy

Sachin Nair,* Jun Gao, Cees Otto, Michael H.G. Duits, and Frieder Mugele*

Cite This: *Anal. Chem.* 2021, 93, 12966−12972

Read Online

ACCESS | Metrics & More | Article Recommendations | Supporting Information

ABSTRACT: We demonstrate how algorithm-improved confocal Raman microscopy (ai-CRM), in combination with chemical enhancement by two-dimensional substrates, can be used as an ultrasensitive detection method for rhodamine (R6G) molecules adsorbed from aqueous solutions. After developing a protocol for laser-induced reduction of graphene oxide, followed by non-invasive Raman imaging, a limit of detection (LOD) of 5×10^{-10} M R6G was achieved using ai-CRM. An equivalent subnanomolar LOD was also achieved on another graphene oxide analogue −UV/ozone-oxidized graphene. These record-breaking detection capabilities also enabled us to study the adsorption kinetics and image the spatial distribution of the adsorbed R6G. These findings indicate a strong potential for algorithm-improved graphene-enhanced Raman spectroscopy as a facile method for detecting, imaging, and quantifying trace amounts of adsorbing molecules on a variety of 2D substrates.

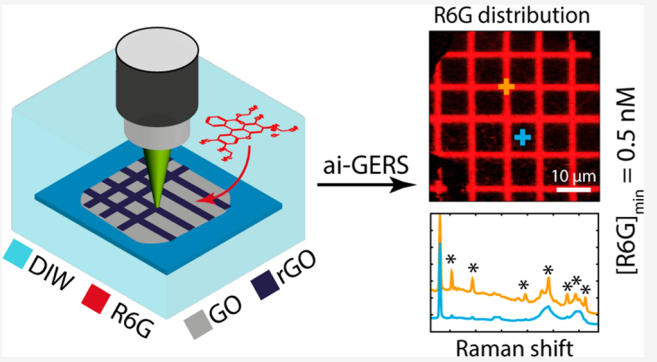

Graphene-enhanced Raman spectroscopy (GERS),[1] a subset of surface-enhanced Raman spectroscopy (SERS),[2,3] refers to the use of graphenic two-dimensional (2D) materials as substrates for enhancing the weak Raman scattering cross-section of adsorbed analyte molecules.[4] Utilizing pristine graphene to suppress the fluorescence of adsorbed rhodamine-6g molecules in resonance Raman spectroscopy,[5] Xi Ling et al. were the first to demonstrate the potential of graphene as a substrate for Raman enhancement.[1] Compared to plasmonic nanoparticle based substrates typically used in SERS, graphenic materials exhibit excellent biocompatibility, chemical inertness, reproducibility, ease of fabrication, and low costs.[6] The atomically flat surface of graphene, endowed with a highly delocalized π-electronic system, provides a very uniform adsorption template for a variety of conjugated probe molecules.[4] Contrary to substrate materials that support surface plasmon resonance in the visible range of the electro-magnetic spectrum, the Raman enhancement in GERS arises from weak surface-analyte charge transfer interactions, also known as the chemical-enhanced mechanism.[7,8] The absence of intense electromagnetic "hot-spots" on graphene and its inert nature also mitigate the photodegradation of the adsorbed molecule, resulting in higher stability of the Raman signal.[9] The aforementioned properties of graphene thus eliminate the problems of irreproducibility and spectral instability that are commonly encountered in SERS.[10] Additionally the chemical enhancement in GERS can be fine-tuned by controlling the interaction distance between the analyte and graphene,[7] the applied-voltage dependent Fermi-level shift of graphene,[11,12] the type of chemical doping,[12−15] the size of the graphitic domains[16] and the molecular structure and energy levels of the analyte.[17]

While initial reports focused on the optimization of graphene as a GERS substrate, similar chemical enhancements have also been reported for other graphenic materials.[18,19] Graphene oxide (GO), the oxidized version of graphene, has certain advantages as a GERS substrate. It can be stably dispersed in water, readily coated on any surface by simple drop-casting and has a rich surface chemistry which can be modulated by varying the degree of oxidation of graphene[20] or the degree of reduction of GO.[21] The controlled reduction of GO to reduced graphene oxide (rGO) not only improves its electrical conductivity due to partial recovery of graphene-like domains,[21,22] but also enables it to act as an efficient GERS substrate.[23,24] rGO can be readily produced from GO by chemical treatment, thermal, or laser annealing.[21] Even though chemical and thermal treatments are most often used to produce rGO, the former can introduce reagent-induced impurities into the rGO lattice,[25] whereas the latter is highly energy intensive.[26] Compared to these, laser-annealed

Received: June 20, 2021
Published: September 14, 2021

fabrication of rGO[27] is facile, energy efficient, and chemical-free, and provides excellent control over the degree of photoreduction by simple tuning of the incident laser dosage.[28,29]

Determining the limit of detection (LOD) of macrocyclic fluorescent molecules like rhodamine-6g (R6G) is one of the most common ways to judge the performance of GERS substrates.[30,31] For instance, a recent study reported the detection and Raman imaging of R6G layers dried onto graphene quantum dots, starting from aqueous droplets with R6G concentrations as low as 1×10^{-9} M.[16] However, most often the probing of trace amounts of analytes in GERS-based chemical and biosensing applications is severely limited by a low signal-to-noise ratio (SNR). As a mitigation, a relatively high laser dosage (exposure time per pixel ~10 s, laser power ~1 mW) is often used when probing low analyte concentrations ($<10^{-6}$ M). However, such a dosage can (a) affect the photostability of the adsorbed fluorescent molecules,[9] (b) compromise the integrity of photosensitive substrates like GO,[32,33] and (c) still involve long exposure times per pixel, making it unattractive to collect large-area Raman maps, as often needed for obtaining statistically sound and reproducible results. Recently it was indicated that such problems could be avoided by using a very low laser dosage combined with so-called algorithm-improved confocal Raman microscopy (ai-CRM).[32] ai-CRM can improve the SNR of collected Raman hyperspectral data sets using a robust and efficient denoising algorithm based on principal component analysis (PCA). Thanks to the improved SNR, the method offers the potential to perform fast and non-invasive Raman imaging and reliable quantification, even for photosensitive systems.

In this work, we show that significant improvements in the detection of R6G molecules on monolayer graphene oxide analogues can be achieved by implementing algorithm-improved GERS. After establishing the range of laser powers where photodamage is avoided, we use ai-GERS to assess the efficiency of photoreduced GO as a Raman enhancement substrate and demonstrate that the limits of detection of R6G molecules on rGO and oxidized graphene substrates are indeed significantly improved. We then use this highly sensitive technique to monitor the in situ adsorption kinetics of R6G on rGO. Lastly, we demonstrate an application of rGO as a sensor for detecting trace adulteration in commercial fruit juice.

EXPERIMENTAL SECTION

Chemicals. A 50 μL GO suspension (2 mg/mL, 22 μm mean diameter flakes, Sigma-Aldrich) was diluted with 30 mL of deionized water (Millipore, resistivity 18.2 MΩ cm). One hundred microliters of this diluted suspension was deposited on 1 × 1 cm plasma-cleaned 300 nm-SiO_2/Si wafers (Okmetic) by drop-casting. After drying in a vacuum oven at 35 °C, the substrate showed partial coverage of single-layer GO flakes, which were optically selected for performing laser writing. Monolayer CVD-grown graphene supported on 1 cm × 1 cm, 300 nm SiO_2/Si substrates (Graphene supermarket, U.S.) were cleaned with deionized water and gently dried under a nitrogen flow. Next, the graphene samples were subjected to oxidation in a UV-Ozone cleaner (Bioforce Nanosciences, ProCleaner Plus) for 5 min, resulting in a large chemical enhancement factor for GERS measurements.[15] The oxidized-graphene (oG) substrates were then used for performing ai-GERS. Aqueous solutions of rhodamine-6g (Merck, 99% dye content) of different concentrations were prepared by diluting a stock solution of 1×10^{-3} M. Commercial fruit-extract based juice was purchased and centrifuged to remove the heavy fruit particulates. The supernatant was then adulterated with R6G such that the final concentration is 50 nM (solvent-juice) for in situ ai-GERS measurements on rGO.

Raman Measurements and Imaging. Raman measurements were carried out using a WiTec alpha 300R Raman microscope equipped with a 532 nm laser. A 600 g/mm (wavenumber range = 0−3710 cm^{-1}) or 1800 g/mm (wavenumber range = 650−1705 cm^{-1}) grating was used as the dispersing element and a CCD camera (1600 × 200 pixels, 16 μm pixel size, Andor Newton) was used for detection of the Raman scattered photons. For performing measurements on the substrate through the ambient deionized water/R6G solution, a 63× water dipping objective (Zeiss W "*N*-Achroplan", Numerical Aperture (NA) 0.9, working distance = 2.4 mm) was chosen. The laser power was measured before the objective (at the turret) using an optical power meter (ThorLabs) and the values are mentioned accordingly.

For a 532 nm laser excitation, the characteristic Raman bands of R6G appear at 610 cm^{-1} (in-plane bending of the xanthene ring), 772 cm^{-1} (out-of-plane bending of C−H) and 1649 cm^{-1} (aromatic C−C stretch). Within the wavenumber resolution of the diffraction grating (2.3 cm^{-1}), the values are in good agreement with previous reports.[1,5] The Si−Si crystalline vibrations from the underlying silicon substrate appear at 520 cm^{-1}. For graphene-oxide (GO), characteristic broad D and G bands appear at 1352 and 1597 cm^{-1} respectively, whereas for graphene the G peak is located at 1590 cm^{-1}.

Laser writing on GO was performed at varying laser power (I_W = 0 to 2 mW) and using an exposure time per pixel, t_W = 0.1 s. Individual square domains of rGO were written over an area of 15 × 15 μm^2 and at a resolution of 20 × 20 pixels. In this manner, six patterns with varying degrees of photoreduction were created on the same GO flake. Multiple writing experiments (n = 4) were performed to ensure reproducibility.

For ai-CRM (ai-GERS), the collected Raman image data set was subjected to cosmic ray removal and principal component analysis (PCA) using home-written codes on MATLAB (version R2017b). Denoising was performed by retaining the first k principal components that explained the maximum variance in the data, during the reconstruction. For more details on the technique, its optimization and the MATLAB code for denoising, readers are encouraged to refer to the original work by Nair et al.[32] Raman imaging was performed by integrating the band of interest in the denoised spectrum for every mapped pixel: from 580 to 670 cm^{-1} for A_{610}, 730−805 cm^{-1} for A_{772} and 1620−1675 cm^{-1} for A_{1649} of R6G, and 480−580 cm^{-1} for A_{Si} of silicon which is used for normalization. Fluorescence area, A_{Fluo} is determined by calculating the area under the curved baseline (excluding band areas) of the Raman spectrum, between 0 and 3692 cm^{-1}. A dark measurement (I_P = 0 mW) was used as the reference background spectrum. Typical Raman maps are made with a resolution of 0.67 μm/pixel, which approximately corresponds to the diffraction-limited spatial resolution of the objective and laser used.

https://doi.org/10.1021/acs.analchem.1c02581
Anal. Chem. 2021, 93, 12966−12972

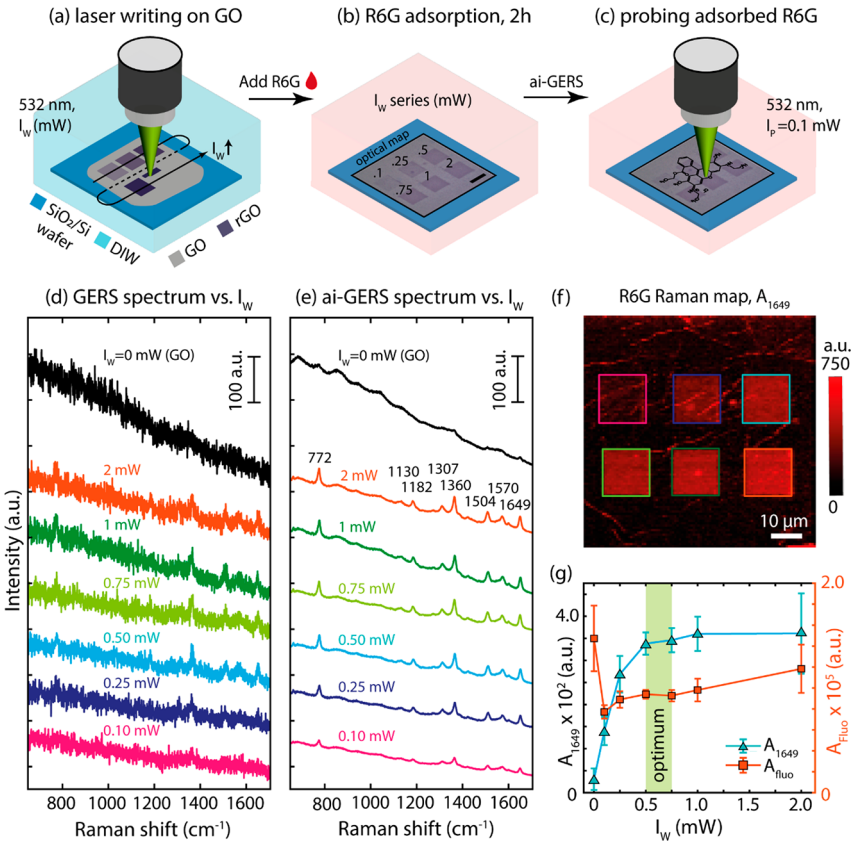

Figure 1. (a–c) Schematic of the subsequent steps in our experiment. (a) in situ laser writing on GO to create rGO domains with varying degree of photoreduction through variation of the writing power I_W, (b) R6G adsorption on the patterned GO flake from a bulk solution with [R6G] = 5×10^{-8} M and (c) measurement of the adsorbed R6G distribution using GERS. (d) representative GERS spectrum (single pixel) as a function of I_W. (e) representative corresponding ai-GERS spectrum vs I_W, showing the improved SNR. The characteristic band positions of R6G are labeled and the spectra have been vertically offset for clarity. (f) Raman map of the adsorbed R6G obtained by integrating across the band at 1649 cm^{-1}. (g) Variation of the mean intensities A_{1649} and A_{Fluo} (integrated over the entire spectrum baseline) with I_W. The optimum I_W (shaded region) is chosen based on A_{1649} being maximal and the spatial variations of A_{1649} and A_{Fluo} (error bars) being minimal. Scale bars: 10 μm.

RESULTS AND DISCUSSION

rGO as a GERS Substrate. rGO substrates were fabricated by in situ photoreduction of GO nanosheets via laser writing.[28,29] First, an as-purchased aqueous GO suspension is drop-cast on a 300 nm SiO_2/Si substrate and dried. The GO coated substrate is then immersed in 20 mL of deionized (DI) water in a liquid cell. A 532 nm laser, focused through a 63x, 0.9 NA, water-dipping objective is used to write 15×15 μm^2 square patterns with different writing powers (I_W − 0.1 to 2 mW), and hence varying rates of photoreduction, on a single GO flake as shown in Figure 1a. AFM characterization of a GO flake patterned in this way shows the presence of a single layer (thickness ∼1.0 nm), with no difference in topography between the rGO and GO regions (refer to Supporting Information (SI) Figure S1a–d). As I_W increases, the D to G Raman band ratio (I_D/I_G) of the laser-illuminated area also increases, which confirms the existence of rGO domains with varying degrees of photoreduction[33] (SI Figure S1e–g). Next (Figure 1b), rhodamine-6g (R6G) is added to the DI water such that the final R6G concentration, [R6G] is 5×10^{-8} M. After an incubation time of 2 h, the spatial distribution of R6G on the substrate is probed using the same optics but a low laser power, I_P = 0.1 mW and an exposure time, t_P = 0.2 s/pixel (Figure 1c). Using the water-immersion objective allows us to probe the analyte adsorption in situ and thereby avoids potential artifacts of common procedures involving intermediate drying steps.

Representative Raman spectra (Figure 1d) obtained from a single pixel over the 15×15 μm^2 reduced areas display a clear dependence on the laser writing power. Clearly, these conventionally obtained GERS spectra suffer from poor SNR, especially when dealing with minimally invasive probing conditions (probe laser dose = 4.89×10^7 J/m^2) and trace analyte concentrations. To tackle this problem, we employ an adaptation of a previously established technique,[32] which we henceforth denote as algorithm-improved graphene-enhanced Raman spectroscopy (ai-GERS). The ai-mode of the technique relies on principal component analysis[34] to reduce the noise of the collected Raman data and to improve the visibility of the low-amplitude bands (compare Figure 1, panel e vs panel d). While the spectrum on unreduced GO is completely dominated by unspecific fluorescence (black curves in Figure 1d,e), the characteristic Raman peaks of R6G are clearly visible above the noise for the different probing areas reduced at variable writing power (colored curves). Probing the reason for observing a higher Raman enhancement on rGO as compared to GO is outside the scope of the current study, but we speculate that this difference could be attributed to a larger adsorption of R6G on rGO, and/or a larger Raman scattering cross-section of the R6G-rGO complex than that of the R6G-GO complex.

https://doi.org/10.1021/acs.analchem.1c02581
Anal. Chem. 2021, 93, 12966−12972

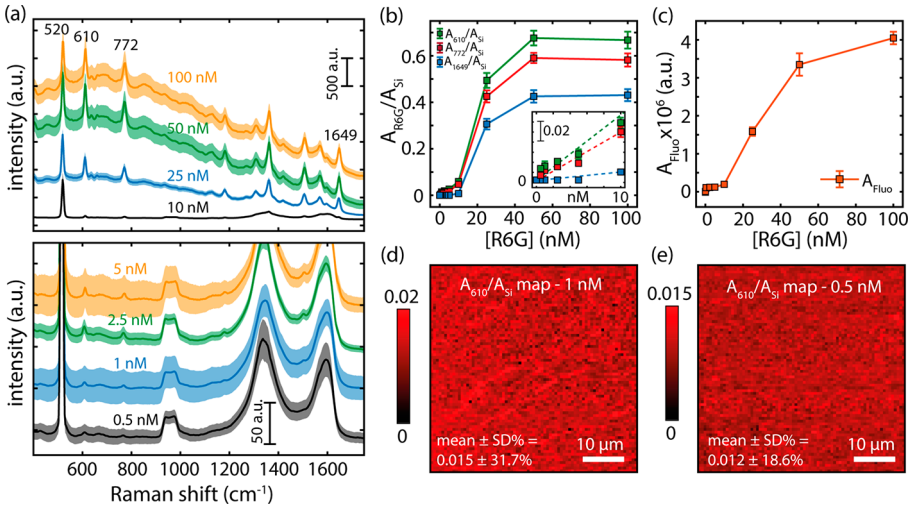

Figure 2. (a) Representative ai-GERS spectra (solid line—mean; shaded background—standard deviation) on rGO for a range of high (top panel) and low (bottom panel) R6G concentrations. The spectra have been offset vertically for clarity. The LOD is determined to be $\approx 5 \times 10^{-10}$ M. (b) Variation of the characteristic R6G Raman bands (A_{610}/A_{Si}, A_{772}/A_{Si}, and A_{1649}/A_{Si}) and (c) fluorescence baseline area (A_{Fluo}) with [R6G]. The inset in (b) shows the linear variation (dashed lines) of the R6G intensities for low concentrations (0—10 nM). (d,e) Corresponding Raman maps obtained by calculating the ratio of A_{610} to A_{Si} at 1×10^{-9} M and 5×10^{-10} M, respectively. The ai-GERS facilitated Raman maps show uniform adsorption of R6G on rGO (relative standard deviations are indicated), even at 5×10^{-10} M.

The enhanced capabilities of ai-GERS are further visualized by the Raman map of the R6G distribution (Figure 1f), obtained by integrating across the 1649 cm^{-1} band of R6G (A_{1649}) for every probed pixel. The mean A_{1649} intensity of R6G is found to increase monotonically for low I_W until it saturates beyond ~0.75 mW (Figure 1g). Interestingly, this trend correlates very well with the increase in the I_D/I_G ratio of (r)GO with I_W (SI Figure S1g). In contrast, the integrated fluorescence intensity (A_{Fluo}) drops by approximately 50% for the lowest I_W and slightly increases again for high I_W. The combined trends indicate an optimum writing power of 0.5—0.75 mW (laser dose = 1.22 to 1.83 $\times 10^8$ J/m^2), generating maximum SNR and minimal spatial variation across the corresponding rGO domains. Technical details of the Raman measurements and vibrational band assignments can be found in the Experimental Section.

Limit of Detection on rGO. Using these optimized reduction conditions (I_W = 0.5 mW), we determined the limit of detection (LOD) of R6G on single rGO layers. To minimize laser-induced changes in the sample while collecting the R6G spectra, we chose a nominal probing laser power, I_P = 0.25 mW and a short exposure time per pixel, t_P = 0.2 s. The corresponding total laser dosage of 1.22 $\times 10^8$ J/m^2 was verified to maintain the photostability (see SI Figure S2) of the adsorbed R6G molecules, while still providing sufficient SNR to probe the adsorption from very dilute solutions ([R6G] $\leq 10^{-7}$ M).

Figure 2 demonstrates the application of rGO as a highly efficient GERS substrate for trace analyte detection. The spatially averaged ai-GERS spectra (solid lines) and their standard deviations (shaded backgrounds) across their respective probed regions (50 μm^2, 75^2 pixels) as a function of bulk R6G concentration (Figure 2a), show that upon decreasing the concentration, the Raman signature band amplitudes of R6G and the fluorescence baseline also reduce. It is important to mention that R6G is a fluorescent molecule and conventional GERS measurements can be difficult to perform at these concentrations, especially when probing in air (lower SNR due to greater refractive index mismatch between air/R6G as compared to water/R6G). However, the improvement in SNR offered by ai-GERS and the in situ conditions of our measurement allow to detect R6G on rGO at bulk concentrations as low as 5×10^{-10} M or 0.5 nM. Xinxin Yu et al. demonstrated Raman signatures of another fluorescent molecule, Rhodamine-B (RhB), on chemically reduced GO down to 5×10^{-8} M.[23] For comparison, we also report the ai-GERS spectrum of 5×10^{-8} M RhB-isothiocyanate on rGO (refer SI Figure S3).

The intensities of the characteristic Raman bands of R6G (A_{610}, A_{772}, and A_{1649}), normalized by the silicon band area at 520 cm^{-1} (A_{Si}), initially increase with the R6G concentration, and reach a plateau beyond ~50 nM (Figure 2b). For the low concentration regime (0—10 nM), the R6G intensities follow a linear trend with [R6G] (inset, Figure 2b). The plateauing at higher concentrations is attributed to the saturation of the R6G adsorption in the first layer in direct contact with the rGO substrate, from where the maximum Raman enhancement in GERS is generally believed to arise.[7] The evolution of the fluorescence baseline area (A_{Fluo}) with [R6G] (Figure 2c) is consistent with this picture, suggesting that the fluorescence suppression by rGO is less efficient beyond the first contacting R6G layer. At the R6G concentrations where the Raman intensities have plateaued, the fluorescence intensities also tend to level off, albeit that a plateau is not reached. The ongoing increase of A_{Fluo} at the highest [R6G] could arise from the (increasingly abundant) free R6G molecules in bulk solution. Figure 2d,e show the corresponding Raman maps (A_{610}/A_{Si}) of the R6G distribution at 1×10^{-9} M and 5×10^{-10} M, respectively (Raman maps at other probed concentrations can be found in SI Figure S4). The uniformity of the distribution (see relative standard deviations) at both concentrations indicates the high affinity and homogeneous adsorption of the R6G molecules on these laser-reduced GO nanosheets, underlining rGO's value as an efficient GERS substrate.

Limit of Detection on Oxidized Graphene. Sung Huh et al.[15] established a protocol for making UV/ozone-oxidized

https://doi.org/10.1021/acs.analchem.1c02581
Anal. Chem. 2021, 93, 12966—12972

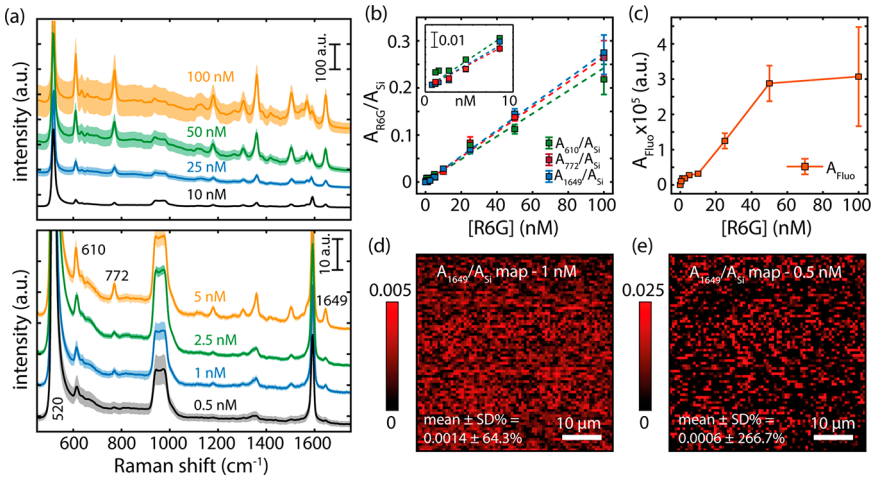

Figure 3. (a) Representative ai-GERS spectra (solid line—mean, shaded background—standard deviation) of R6G on oxidized-graphene (oG) substrates for a range of high (top panel) and low (bottom panel) R6G concentrations. The spectra have been offset vertically for clarity. The experimental LOD is $\approx 5 \times 10^{-10}$ M. (b) Variation of the characteristic R6G Raman bands (A_{610}/A_{Si}, A_{772}/A_{Si} and A_{1649}/A_{Si}) and (c) fluorescence background (A_{Fluo}) with [R6G]. The inset in (b) shows the variation of the R6G intensities for low concentrations (0–10 nM). (d,e) Corresponding Raman maps obtained by calculating A_{1649}/A_{Si} at 1×10^{-9} M and 5×10^{-10} M, respectively. The ai-GERS-facilitated Raman maps help to visualize submonolayer coverage of R6G on oG for these low bulk concentrations.

CVD-graphene substrates which give a 10-fold stronger Raman enhancement as compared to their unoxidized counterpart. In their work, CVD grown graphene samples supported on a SiO_2/Si substrate were subjected to UV-Ozone treatment for 5 min and directly used as GERS substrates. Following the same protocol, we use these oxidized graphene (oG) substrates to demonstrate the efficiency of ai-GERS for sub-nM R6G detection and imaging. The variation of the spatially averaged (50 μm^2, 75^2 pixels) ai-GERS spectra vs the bulk [R6G] on oG substrates (Figure 3a) show that the characteristic R6G bands can be detected for concentrations as low as 5×10^{-10} M, lower than any previously reported LOD for this system. Recently, Donghua Liu et al. detected R6G layers dried onto ultraclean graphene quantum dots (GQD) substrates from a solution at 1×10^{-9} M.[16] Note that, while the absolute LOD is thus reduced by a factor of 2, our improvement is also achieved using commercially available materials with minimal preparation effort. Furthermore, our in situ measurements are performed while the substrate remains in contact with a fluid of fixed specified concentration, thereby avoiding possible up-concentration effects due to drying (leading to an overestimation of the actual LOD; see SI Figure S5 for the Raman spectrum of a dried 1×10^{-11} M R6G droplet on oG).

Quantification of the R6G band intensities as a function of [R6G] (Figure 3b) displays a linear trend throughout the probed concentration range, in contrast to rGO where such linearity was only observed for lower concentrations (inset, Figure 2b). Following the suggestion of Xi Ling et al.[1] who reported submonolayer adsorption for bulk concentrations below 8×10^{-7} M, we attribute the linear behavior in Figure 3b to incomplete adsorption within the first monolayer (for the investigated concentration range). It also turns out that the A_{R6G}/A_{Si} band ratios are significantly lower on oG as compared to the rGO case. The evolution of the fluorescence area with [R6G] on oG, however, behaves similarly to the rGO case (compare Figure 3c with Figure 2c). Within the (diffraction-limited) spatial resolution, Figure 3d,e further supports the picture of partial coverage on the oG substrates at bulk R6G concentrations of 1×10^{-9} M and 5×10^{-10} M, respectively (for Raman maps at other R6G concentrations, refer SI Figure S6). ai-GERS-facilitated Raman imaging thus provides unprecedented insights into submonolayer adsorption.

Applications of ai-GERS. The in situ nature of the measurement allows us to directly probe the adsorption kinetics of R6G on single-flake rGO (in contrast to GERS studies that examine dried analyte layers in air). Dynamic *xy*-Raman imaging (50×50 um^2, 50×50 pixels, $I_P = 0.25$ mW and $t_P = 0.05$ s/pixel) for 175 min shows the gradual R6G adsorption onto rGO (created with $I_W = 0.5$ mW) upon exposure to a 50 nM solution. The spatially averaged spectrum displays an increase in the R6G fingerprint band amplitudes (Figure 4a), leading to an S-shaped "adsorption curve" of A_{610}/A_{Si} versus time (Figure 4b). A steady state appears to be reached after ~2 h. For the evolution of the Raman maps, see SI Figure S7.

As another application, we analyzed the presence of trace amounts of R6G that had been added to a commercial fruit juice. Xanthene-based dyes like Rhodamine are widely used in the textile and leather industries as colorants, but have been shown to be carcinogenic and cytotoxic.[35] In addition to the harmful health effects when reaching drinking water,[36] there are also growing concerns about Rhodamine dyes being used as illegal food colorants.[37,38] Here, we demonstrate the ability of in situ ai-GERS to detect and visualize 50 nM of R6G dissolved in an as-purchased fruit juice (inset, Figure 4c). To this end, we utilize rGO ($I_W = 0.5$ mW) as a GERS substrate, and compare the Raman responses of the original (i.e., blank) and adulterated juices. The blank juice (Figure 4c, black curve) shows no particular Raman features except for the Si and rGO bands from the substrate, whereas the adulterated one (magenta curve) clearly shows a fluorescence baseline and characteristic R6G bands (denoted by *). The Raman map of the adsorbed R6G (A_{1649}/A_{Si}) from the adulterated juice is shown in Figure 4d. These results clearly highlight the capabilities of in situ ai-GERS for detecting trace analytes in complex solutions. Both the high affinity of the conjugated R6G molecule to adsorb onto the rGO lattice and the algorithm-improved SNR enhancement of Raman signals are

https://doi.org/10.1021/acs.analchem.1c02581
Anal. Chem. 2021, 93, 12966–12972

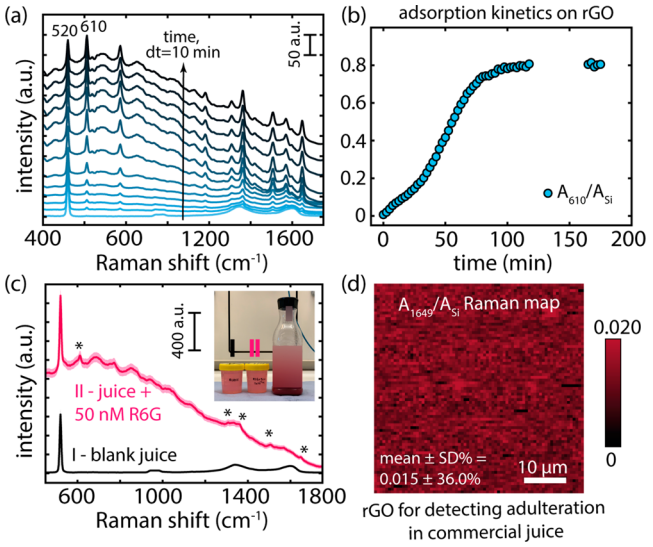

Figure 4. (a) Evolution of the spatially averaged ai-GERS spectrum of R6G adsorbing onto rGO after 50 nM R6G addition at $t = 0$ min. The spectra have been offset vertically for clarity. (b) Adsorption curve depicting the growth of the A_{610}/A_{Si} ratio over time. A steady state is reached after ~2 h. (c) Comparison of the ai-GERS response of an original juice vs one that was adulterated with 50 nM of R6G, on rGO. Inset shows the photograph of the juice and the two solutions: *I*, blank and II, adulterated juice. (d) Raman map of (A_{1649}/A_{Si}), reflecting the R6G adsorbed from the adulterated juice on rGO.

pertinent to the ultrasensitive detection of analytes on graphene oxide analogues.

CONCLUSIONS

In summary, we utilized an algorithm-improved (ai-) mode of Raman imaging[32] to considerably improve the sensitivity of analyte detection in the field of graphene-enhanced Raman spectroscopy (GERS). We demonstrated that reduced graphene oxide (rGO), obtained via laser writing, is a far superior GERS substrate as compared to its unreduced counterpart in terms of fluorescence suppression and Raman enhancement. Our results show the capability of ai-GERS in improving the limit of detection (LOD) of rhodamine-6g layers adsorbed onto single rGO flakes, to bulk R6G concentrations as low as 5×10^{-10} M. Keeping in line with the practical necessity of avoiding complex substrate fabrication for sensitive analyte sensing, we also report an improved LOD of 5×10^{-10} M for R6G on facile oxidized graphene (oG) samples. ai-GERS facilitated imaging provides direct and non-invasive visualization of the adsorbed analyte distribution, even at subnanomolar concentrations. From a practical standpoint, we show the advantage of in situ ai-GERS measurements to monitor and image the adsorption kinetics of R6G on rGO, and also show the capability of rGO as a sensor for detecting trace adulteration in a commercial juice. We believe that ai-GERS could potentially improve low concentration analyte detection, quantification and imaging on various substrates useful for chemical and biosensing applications.[30]

ASSOCIATED CONTENT

Supporting Information

The Supporting Information is available free of charge at https://pubs.acs.org/doi/10.1021/acs.analchem.1c02581.

AFM and Raman characterization of a photoreduced GO flake (Figure S1), Photostability measurements of R6G on rGO (Figure S2), ai-GERS spectrum of Rhodamine-B isothiocyanate (RhB-ITC) on rGO (Figure S3), Raman maps of R6G on rGO at other probed concentrations (Figure S4), ai-GERS spectrum of a dried 1×10^{-11} M R6G droplet on oxidized-graphene (oG) (Figure S5), Raman maps of R6G on oG for 6 concentrations (Figure S6), and Evolution of the R6G distribution for probing adsorption kinetics (Figure S7) (PDF)

AUTHOR INFORMATION

Corresponding Authors

Sachin Nair − *Physics of Complex Fluids Group and MESA+ Institute, University of Twente, 7500 AE Enschede, The Netherlands;* orcid.org/0000-0002-4413-6116; Email: s.s.nair@utwente.nl

Frieder Mugele − *Physics of Complex Fluids Group and MESA+ Institute, University of Twente, 7500 AE Enschede, The Netherlands;* orcid.org/0000-0003-3824-3617; Email: f.mugele@utwente.nl

Authors

Jun Gao − *Qingdao Institute of Bioenergy and Bioprocess Technology, Chinese Academy of Sciences, Laoshan District, Qingdao 266101, P. R. China;* orcid.org/0000-0003-2106-3134

Cees Otto − *Medical Cell Bio Physics Group and TechMed Centre, University of Twente, 7500 AE Enschede, The Netherlands*

Michael H.G. Duits − *Physics of Complex Fluids Group and MESA+ Institute, University of Twente, 7500 AE Enschede, The Netherlands;* orcid.org/0000-0003-1412-4955

Complete contact information is available at: https://pubs.acs.org/10.1021/acs.analchem.1c02581

Notes

The authors declare no competing financial interest.

ACKNOWLEDGMENTS

This work is part of the research program Rock-on-a-Chip with project number i40, which is partly financed by The Netherlands Organization for Scientific Research (NWO) and the Exploratory Research (ExploRe) program of BP plc. We thank B. Ilhan and S. Kumar for carrying out the in situ AFM imaging of (r)GO flakes.

REFERENCES

(1) Ling, X.; Xie, L.; Fang, Y.; Xu, H.; Zhang, H.; Kong, J.; Dresselhaus, M. S.; Zhang, J.; Liu, Z. *Nano Lett.* **2010**, *10* (2), 553−561.
(2) Fleischmann, M.; Hendra, P. J.; McQuillan, A. J. *Chem. Phys. Lett.* **1974**, *26* (2), 163−166.
(3) Campion, A.; Kambhampati, P. *Chem. Soc. Rev.* **1998**, *27* (4), 241−250.
(4) Ling, X.; Huang, S.; Deng, S.; Mao, N.; Kong, J.; Dresselhaus, M. S.; Zhang, J. *Acc. Chem. Res.* **2015**, *48* (7), 1862−1870.
(5) Xie, L.; Ling, X.; Fang, Y.; Zhang, J.; Liu, Z. *J. Am. Chem. Soc.* **2009**, *131* (29), 9890−9891.
(6) Xu, W.; Mao, N.; Zhang, J. *Small* **2013**, *9* (8), 1206−1224.
(7) Ling, X.; Zhang, J. *Small* **2010**, *6* (18), 2020−2025.
(8) Tantiwanichapan, K.; Wang, X.; Durmaz, H.; Li, Y.; Swan, A. K.; Paiella, R. *ACS Photonics* **2017**, *4* (8), 2011−2017.

(9) Zhao, Y.; Xie, Y.; Bao, Z.; Tsang, Y. H.; Xie, L.; Chai, Y. *J. Phys. Chem. C* **2014**, *118* (22), 11827−11832.
(10) Lin, X.-M.; Cui, Y.; Xu, Y.-H.; Ren, B.; Tian, Z.-Q. *Anal. Bioanal. Chem.* **2009**, *394* (7), 1729−1745.
(11) Xu, H.; Xie, L.; Zhang, H.; Zhang, J. *ACS Nano* **2011**, *5* (7), 5338−5344.
(12) Hao, Q.; Morton, S. M.; Wang, B.; Zhao, Y.; Jensen, L.; Jun Huang, T. *Appl. Phys. Lett.* **2013**, *102* (1), 011102.
(13) Valeš, V.; Drogowska-Horná, K.; Guerra, V. L.; Kalbáč, M. *Sci. Rep.* **2020**, *10* (1), 1−9.
(14) Feng, S.; dos Santos, M. C.; Carvalho, B. R.; Lv, R.; Li, Q.; Fujisawa, K.; Elías, A. L.; Lei, Y.; Perea-López, N.; Endo, M. *Science advances* **2016**, *2* (7), e1600322.
(15) Huh, S.; Park, J.; Kim, Y. S.; Kim, K. S.; Hong, B. H.; Nam, J.-M. *ACS Nano* **2011**, *5* (12), 9799−9806.
(16) Liu, D.; Chen, X.; Hu, Y.; Sun, T.; Song, Z.; Zheng, Y.; Cao, Y.; Cai, Z.; Cao, M.; Peng, L. *Nat. Commun.* **2018**, *9* (1), 1−10.
(17) Huang, S.; Ling, X.; Liang, L.; Song, Y.; Fang, W.; Zhang, J.; Kong, J.; Meunier, V.; Dresselhaus, M. S. *Nano Lett.* **2015**, *15* (5), 2892−2901.
(18) Sil, S.; Kuhar, N.; Acharya, S.; Umapathy, S. *Sci. Rep.* **2013**, *3*, 3336.
(19) Yang, H.; Hu, H.; Ni, Z.; Poh, C. K.; Cong, C.; Lin, J.; Yu, T. *Carbon* **2013**, *62*, 422−429.
(20) Krishnamoorthy, K.; Veerapandian, M.; Yun, K.; Kim, S.-J. *Carbon* **2013**, *53*, 38−49.
(21) Pei, S.; Cheng, H.-M. *Carbon* **2012**, *50* (9), 3210−3228.
(22) Wei, Z.; Wang, D.; Kim, S.; Kim, S.-Y.; Hu, Y.; Yakes, M. K.; Laracuente, A. R.; Dai, Z.; Marder, S. R.; Berger, C. *Science* **2010**, *328* (5984), 1373−1376.
(23) Yu, X.; Cai, H.; Zhang, W.; Li, X.; Pan, N.; Luo, Y.; Wang, X.; Hou, J. *ACS Nano* **2011**, *5* (2), 952−958.
(24) Wang, L.; Zhang, Y.; Yang, Y.; Zhang, J. *Materials* **2018**, *11* (7), 1199.
(25) Chua, C. K.; Pumera, M. *Chem. Soc. Rev.* **2014**, *43* (1), 291−312.
(26) Zhang, P.; Li, Z.; Zhang, S.; Shao, G. *Energy & Environmental Materials* **2018**, *1* (1), 5−12.
(27) Zhang, Y. L.; Guo, L.; Xia, H.; Chen, Q. D.; Feng, J.; Sun, H. B. *Adv. Opt. Mater.* **2014**, *2* (1), 10−28.
(28) Ma, B.; Rodriguez, R. D.; Ruban, A.; Pavlov, S.; Sheremet, E. *Phys. Chem. Chem. Phys.* **2019**, *21* (19), 10125−10134.
(29) Arul, R.; Oosterbeek, R. N.; Robertson, J.; Xu, G.; Jin, J.; Simpson, M. C. *Carbon* **2016**, *99*, 423−431.
(30) Wang, Z.; Wu, S.; Ciacchi, L. C.; Wei, G. *Analyst* **2018**, *143* (21), 5074−5089.
(31) Silver, A.; Kitadai, H.; Liu, H.; Granzier-Nakajima, T.; Terrones, M.; Ling, X.; Huang, S. *Nanomaterials* **2019**, *9* (4), 516.
(32) Nair, S.; Gao, J.; Yao, Q.; Duits, M. H.; Otto, C.; Mugele, F., Algorithm-improved high speed and non-invasive confocal Raman imaging of two-dimensional materials. *National Science Review* **2020**.7620
(33) Mehta, J. S.; Faucett, A. C.; Sharma, A.; Mativetsky, J. M. *J. Phys. Chem. C* **2017**, *121* (30), 16584−16591.
(34) Abdi, H.; Williams, L. J. *Wiley interdisciplinary reviews: computational statistics* **2010**, *2* (4), 433−459.
(35) Nestmann, E. R.; Douglas, G. R.; Matula, T. I.; Grant, C. E.; Kowbel, D. J. *Cancer Res.* **1979**, *39* (11), 4412−4417.
(36) Jain, R.; Mathur, M.; Sikarwar, S.; Mittal, A. *J. Environ. Manage.* **2007**, *85* (4), 956−964.
(37) Qi, P.; Lin, Z.; Li, J.; Wang, C.; Meng, W.; Hong, H.; Zhang, X. *Food Chem.* **2014**, *164*, 98−103.
(38) Tian, H.; Zhang, N.; Tong, L.; Zhang, J. *Small Methods* **2017**, *1* (6), 1700126.

https://doi.org/10.1021/acs.analchem.1c02581
Anal. Chem. 2021, 93, 12966−12972